

GraViti: Graph-Level Variational Autoencoders with Relaxed Permutation Invariance

Roman Bresson

Mohamed bin Zayed University of Artificial Intelligence

Konstantinos Divriotis

Mohamed bin Zayed University of Artificial Intelligence

Johannes F. Lutzeyer

LIX, CNRS, École Polytechnique, IP Paris

Iakovos Evdaimon

LIX, CNRS, École Polytechnique, IP Paris

Michalis Vazirgiannis

Mohamed bin Zayed University of Artificial Intelligence

LIX, CNRS, École Polytechnique, IP Paris

Abstract

We introduce GraViti, a transformer-based graph-level variational autoencoder that maps entire graphs to compact latent vectors. This design produces a true graph-level latent space that supports smooth interpolation, property-guided search, and other downstream tasks beyond the constraints of node-level embeddings. On molecular benchmarks, GraViti learns to decode valid samples that follow the chemical constraints present in the training data, showing that the model recovers domain rules directly from graph-level representations. We also show that, in domains where a reliable canonical node ordering exists such as molecules or bayesian networks, enforcing permutation invariance can prove detrimental for consistent reconstruction. GraViti achieves state-of-the-art reconstruction accuracy on large datasets, and provides solid generative performance. Its single-step decoding offers a lightweight alternative to more complex generation pipelines while maintaining practical sample quality.

1 Introduction

Autoencoders [1] are unsupervised learning models designed to learn compact representations of complex data. They consist of two components: an encoder that maps an input data point (such as an image, or in our case a graph) into a low-dimensional latent vector, and a decoder that reconstructs the original data from this latent code. The model is trained end-to-end by minimizing the difference between the input and its reconstruction. This training process forces the latent representation to capture the essential structure of the data while discarding redundancy and noise. As a result, autoencoders are widely used for tasks such as denoising, compression, and extracting meaningful features that can support downstream applications [2, 3].

To enforce structure on the latent representations, variational autoencoders [4] constrain the distribution of all data point embeddings z to match a fixed distribution (usually normal) through minimizing a KL-divergence term. This contributes to regularizing the model to obtain more meaningful latent representations, as well as enabling sampling capabilities.

Despite extensive work on autoencoders across modalities [5], graph-level autoencoding remains comparatively underexplored. Most approaches covering graph-oriented AE and VAEs do so at node-level. The early approach by Kipf et al. [6] encodes a graph of N -nodes into N latent vectors, each encoding one node’s information, and the decoder recovers the adjacency matrix. More recent methods still follow this approach [7, 8, 9], which amounts to squeezing the adjacency information of each node inside its representation. This approach significantly limits the ability to capture meaningful distances between graphs. Because the latent space is defined at the node level and depends on the arbitrary ordering

of nodes, two isomorphic graphs can map to entirely different sets of latent vectors (up to a permutation). As a result, node-level VAEs cannot define distances between graphs or capture graph-level manifolds [10].

Alternatively, graph-level autoencoders (which encode an entire graph in a single latent representation) remain under-explored, with PIGVAE [11] and GRALE [12] being notable exceptions which will be further discussed in this work. This can be traced to several core challenges inherent to their design. First, the encoder must be permutation-invariant, since node order is arbitrary while graph structure is not; without this property, the latent vector risks encoding artefacts of node indexing rather than genuine topology. Second, the model must handle variable graph sizes: the encoder must accept graphs of arbitrary cardinality, and the decoder must expand a single latent vector into a graph whose size is not known in advance, a requirement that makes graph-level decoding substantially more complex than its node-level counterpart.

In this work, we introduce **GraViti**, a graph-level VAE that encodes entire graphs into single latent vectors using a graph-transformer backbone. Our contributions are threefold. First, we propose a scalable architecture that achieves state-of-the-art reconstruction accuracy on large graph datasets. Second, we show that the learned latent space is well structured and faithfully reflects the underlying domain constraints; on molecular benchmarks, it not only supports interpolation, controlled editing, and property-driven optimization, but also recovers well-established chemical phenomena. Third, we demonstrate empirically that permutation invariance can be relaxed for reconstruction when a consistent canonical node ordering is available, an assumption that holds in domains such as molecular graphs and Bayesian networks.

2 Background and state of the art

Permutation-invariant encoding of size-varying graphs Early graph neural networks address the issue of finding a permutation-equivariant node-representation through message passing with permutation-invariant aggregation [13, 14], including attention-based aggregators [15], allowing neighbor-specific information transmission [16, 17].

Due to the limited expressivity of message-passing GNNs [14], graph transformers [18, 19] were introduced, allowing all nodes to attend to all other nodes, at the cost of computing the full attention matrix. Like in language processing, a positional encoding now represents the structural information [20, 21]. Common choices include Laplacian eigenvectors, random-walk features, or shortest-path distances. Hybrid approaches, such as GraphGPS [22] or SAT [23] combine transformers with message-passing to balance efficiency and flexibility. Both message-passing GNNs and graph transformers operate directly on sets of nodes and edges, which ensures permutation-equivariant node representations and allows them to process graphs of arbitrary size without requiring a fixed ordering. This makes them suitable graph-encoders, as used in the original Graph VAE [6]. For graph-oriented tasks, a permutation-invariant pooling operation then produces a graph-level representation, although this often discards substantial structural information [24].

Size-varying and permutation-invariant decoding Graph (variational) autoencoders must reconstruct a graph whose size is not known in advance, and must determine how each reconstructed node corresponds to each input node in order to compute the reconstruction loss. Node-level approaches handle this naturally, since the encoder produces one latent vector per input node. The decoder then reconstructs the adjacency matrix and node attributes in a fixed order, so the correspondence between input and output nodes is implicit in the node indexing. Well-used decoders include inner-product or MLP [6]. Message passing can then be used for refinement [25].

Graph-level autoencoders have several ways of addressing the permutation-dependent reconstruction loss. One common approach is graph matching [26, 27], which finds an optimal node alignment between the input and reconstructed graph. This is theoretically sound, but the optimization step is computationally expensive, typically requiring approximate solvers for quadratic assignment problems. More recently, PIGVAE [11] introduced a learnable matching module that predicts a relaxed permutation matrix, obtained by sorting node embeddings. While this bypasses the quadratic assignment problem, it provides only a limited form of alignment. GRALE [12] extends this idea by combining an optimal-transport-based reconstruction loss with a Sinkhorn-based matcher, producing a full doubly stochastic alignment matrix and significantly improving stability and expressivity.

Addressing variable graph sizes is commonly approached through padding [12, 28], in the same way as

in natural language processing with transformers [15], where all graphs are resized to a fixed maximum size, often by introducing a “dummy node” class to complete the node feature matrix. The decoder then predicts a graph of maximal size along with a node mask indicating which nodes belong to the reconstructed graph. However, these strategies introduce two major limitations: (i) enforcing a fixed maximum graph size restricts the model’s ability to generalize to larger graphs, and (ii) introducing a dummy node class biases the node classification task by adding an artificial class that does not correspond to any real element. PIGVAE uses an arguably more flexible approach by using a sequence transformer on duplicates of the graph representation, differentiated by sinusoidal positional encoding. This allows to avoid both using a maximum size and using a dummy node, simply masking non-existing nodes. The size is predicted by an MLP from the latent representation.

Overall, existing graph autoencoding methods face a fundamental trade-off. Node-level approaches scale well but fail to produce coherent graph-level latent spaces, while graph-level methods rely on costly permutation-invariant matching procedures that limit scalability. This gap motivates the need for architectures that can learn meaningful graph-level representations without incurring expensive alignment steps, while still remaining expressive and scalable to large datasets.

3 The GraViti architecture

Graph representation Let N denote the size of the graph (i.e., the number of nodes). In this work, we assume that graphs have discrete node classes and edge classes instead of continuous feature (e.g. atom classes, color). A graph is represented by two objects. First is its node classes matrix $X \in \mathbb{R}^{N \times n_c}$ where n_c is the number of node classes and X_i is the one-hot encoding of the i -th node’s class. Importantly, we do not introduce a “dummy node” class; all classes correspond to real nodes. Then $E \in \mathbb{R}^{N \times N \times n_e}$ is the edge class tensor, where n_e is the number of edge classes, including both actual edge types and an additional class representing “no edge”.

To enrich the graph representation, we compute directly from the graph a global feature vector $y \in \mathbb{R}^{d_y}$ containing graph-level information. In practice, $d_y = n_c + n_e + 1$, and y encodes the count of each node and edge type, as well as the graph size. We also compute $P \in \mathbb{R}^{N \times d_p}$, the positional encodings for the nodes, obtained by concatenating Laplacian positional encodings and random walk positional encodings. These inject structural information into the graph transformer.

Finally, when relevant for the field, we also exploit a matrix of node-specific features derived from domain knowledge $K \in \mathbb{R}^{N \times d_k}$. For molecular datasets, these include atomic properties such as atomic number, atomic mass, valence electrons, and electronegativity.

Since training involves batching, all graphs in a batch must share the same size. To achieve this, we pad all graphs to reach the size of the largest graph in the batch, extending X , P , K , and E accordingly. This padding has no semantic meaning, and the model is designed to ignore it entirely. The padded size of the input does not influence the decoder or model size in any way. The model is illustrated in figure 1; the letters in paragraph titles refer to the respective components on the figure.

Encoding node, edge, and global representation (A) Our encoder maps a triplet X, E, y (optionally P and K) to a mean and standard deviation $z_\mu, z_\sigma \in \mathbb{R}^{d_z}$ where d_z is the latent dimension.

At first, the node representation matrix is expanded into X_{emb} by concatenating a learned shallow embedding of the node class, both positional encoding (laplacian and random-walk) processed through a dedicated linear layer and optionally node attributes processed through a dedicated linear layer. Edge representations are obtained via a learned embedding layer of their discrete classes, producing E_{emb} . The global feature vector y is projected through a linear layer into y_{emb} .

All three tensors ($X_{\text{emb}}, E_{\text{emb}}, y_{\text{emb}}$) undergo layer normalization and are updated through multiple graph transformer layers, yielding $X_{\text{rep}}, E_{\text{rep}}$, and y_{rep} . This step uses the specific graph transformer architecture introduced in DiGress [29] and updated in CatFlow [30]. This design enables simultaneous updates of node, edge, and graph-level features while ensuring permutation-equivariance.

Encoder readout (B) Traditional readout functions for graph-level representations (such as sum, mean, or max pooling) are permutation-invariant at the cost of a large quantity of information. To ensure a highly expressive latent space, we adopt a sequence transformer-based readout mechanism.

Unlike GRALE, which applies a transformer solely on node embeddings, our approach incorporates nodes, edges, and global features into the readout to prevent overloading node embeddings. Specifically, the readout consists of two parallel sequence-decoder transformers: one for nodes and one for edges.

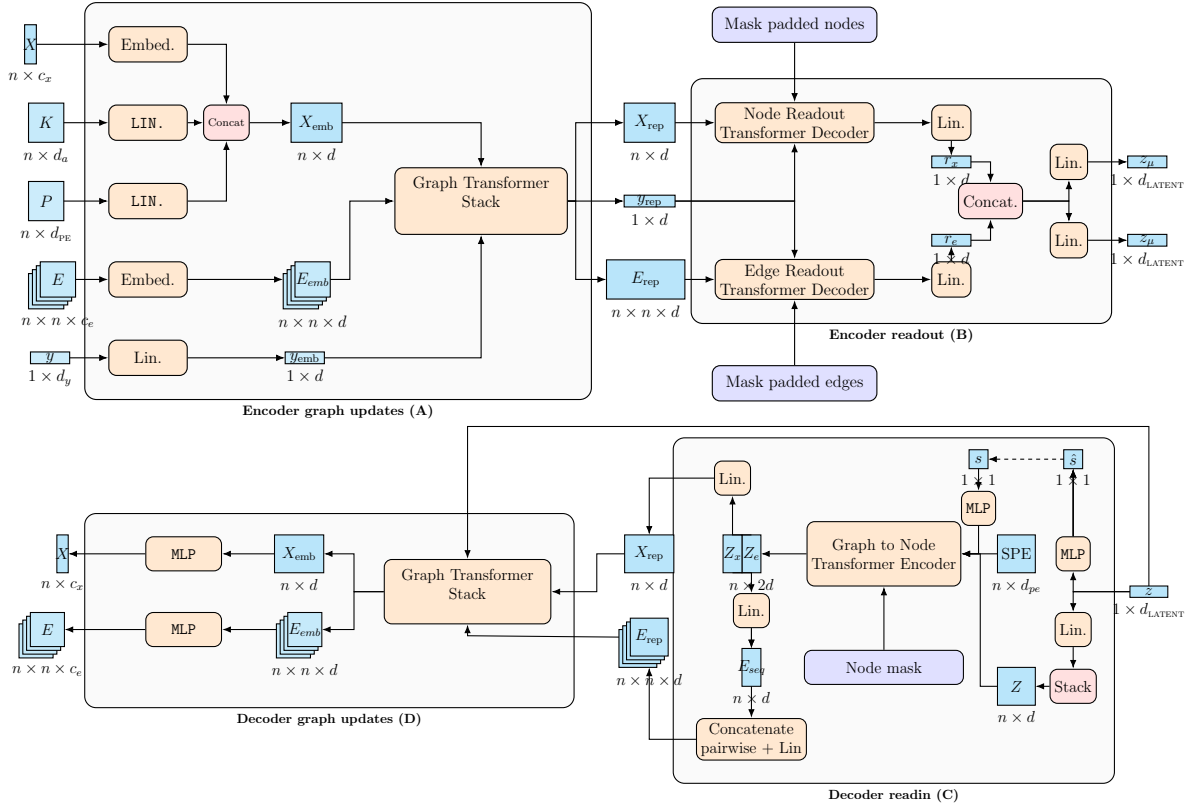


Figure 1: The architecture of our model. The data space is on the left, while the latent space is on the right. Encoder on top reads left to right, decoder reads right to left.

Both transformers are masked to ignore padded nodes and edges. y_{rep} serves as the target for both transformers, injecting global context into the readout.

Since positional encodings are omitted at this stage, the inherent permutation invariance of the sequence transformer guarantees that the output is independent of node ordering. Finally, node and edge outputs are normalized independently and projected through linear layers to produce the graph-level representation. This one can be either a single vector (classic autoencoder case) or a pair of same-sized vectors (in the variational case).

Graph size prediction (C) One crucial information required to reconstruct the graph is its size, which needs to be recovered from the latent representation. We make the design choice of disentangling this crucial structural information from the rest of the latent representation by forcing the model to encode it in only the first d_s dimensions of the latent space. The log-size \hat{s} is then predicted by an MLP. In order for the decoding process to leverage the size information, we use another MLP to re-encode the log-size s into d_s dimensions that replace the corresponding latent features. During training, no gradient flows between \hat{s} and s . The predicted log-size \hat{s} is optimized via a smooth L1 loss against the ground-truth log-size, while the ground-truth value s is directly reinjected into the latent representation. This ensures that the corresponding latent dimensions encode size information exclusively, rather than relying on indirect supervision through masking.

Decoding graph-level into node-level representation (C) The first module of our decoder has to invert the readout function, i.e. obtain node representations from graph representations. Similarly to PIGVAE we first broadcast the graph-level information into a node-wise representation. This is done by simply duplicating our graph-level representation (i.e. the latent representation projected through a linear layer) N times. We therefore obtain a sequence of N identical vectors of dimension D . In order to break the symmetries and allow the transformer to differentiate between these pseudo-tokens, we add sinusoidal positional encoding to the sequence. During training, N is determined as the ground truth size, which is also used for reinjection. During inference, N is $\text{round}(\exp(\hat{s}))$.

This sequence is then updated into another $N \times D$ sequence through a sequence transformer encoder,

matching our readout. We then split this sequence width-wise into two sequences of size $N \times \frac{D}{2}$, a node-oriented sequence X_x and an edge-oriented sequence X_e . We create an edge-feature matrix ϕ_e by concatenating the rows of X_e in pairs: $\phi_{e,(i,j)} = X_{e,i}|X_{e,j}$; finally, symmetric edge-feature Φ_e matrix is obtained as $\Phi_{e,(i,j)} = \frac{1}{2}(\phi_{e,(i,j)} + \phi_{e,(j,i)}) \in \mathbb{R}^{n \times n \times D}$. In parallel, we create a node features matrix $\phi_x \in \mathbb{R}^{n \times D}$.

Updating and refining the graph (D) We update the obtained graph through another graph transformer, with similar architecture as that of the encoder. Finally, we apply an MLP to the nodes and one to the edges as a final prediction head. In our case, those are classifiers. We only reconstruct X and E , which is all that is needed for a graph. Also note that the size is predicted, and there is therefore no need to predict an extra dummy node class.

The model is trained following the standard VAE objective, using a focal loss [31] for all node and edge predictions. This choice is motivated by the strong class imbalance. A KL term regularizes the latent variables toward a normal prior. Details of the loss formulation are provided in Appendix B.

4 Comparison to GRALE and PIGVAE

We clarify here the difference between GRALE, PIGVAE and GraViti.

Loss function Both GRALE and PIGVAE leverage a permutation-invariant scheme for their loss functions, allowing to reconstruct the graph in any order while still obtaining a relevant reconstruction loss: PIGVAE predicts a permutation matrix obtained through a solver, while GRALE iterates upon this by using a Sinkhorn matcher to obtain a relaxed permutation matrix, and using the Any2Graph loss [32] on the soft assignment. While these approaches are elegant and well-suited to fully general graph settings, this incurs a significant computational overhead (at least cubic for both approaches). In contrast, our model relies on a simpler reconstruction objective made possible by the use of a consistent node ordering, allowing a quadratic complexity. In practice, this results in improved reconstruction quality on the benchmarks we consider, especially as graph size increases.

Graph size flexibility GRALE decodes graphs by iteratively refining a learned node and edge representation of fixed maximal size, with additional nodes pruned via a learned mask. This mechanism inherently enforces an upper bound on the size of generated graphs. In contrast, our approach, like PIGVAE, does not impose such a limit: the graph-level latent is replicated to the desired number of nodes, and continuous sequence-based positional encodings are used to distinguish node-level embeddings. As a result, the model architecture is independent of graph size, although computational cost for full attention naturally scales with it.

Variational component Similar to PIGVAE, our method follows a fully variational formulation, enabling likelihood-based training and explicit regularization of the latent space. Unlike GRALE, which relies on a tokenized latent representation, we operate in a continuous latent space. In practice, this enables a well-structured latent, unlocking in particular generative and editing capabilities.

5 Experimental results

5.1 Experimental setting

A prominent application domain for graph-level representation learning is computational chemistry, where molecules are naturally represented as attributed graphs of atoms and bonds. We consider two benchmark datasets: QM9 [33], a dataset of approximately 130,000 molecules containing up to 9 heavy atoms, and PubChem [34]. Following GRALE, we focus on the PubChem16 and PubChem32 subsets, comprising approximately 13 million and 74 million molecules with up to 16 and 32 heavy atoms, respectively. Detailed dataset statistics are provided in appendix A. As is standard in molecular graph modeling, we remove explicit hydrogen atoms [35, 36, 30, 37]. The resulting graphs contain four bond types: single, double, triple, and aromatic. We also consider general graphs with the COLORING dataset, and bayesian networks for downstream tasks.

Extra loss terms for molecules In the case of molecules, the graph representation (atom-types/bond-type) does not contain all of the relevant information when using the aromatic representation. To alleviate this ambiguity, we also predict the formal charge and number of bonded hydrogen atoms for all atoms that are part of an aromatic ring using two extra prediction heads.

Table 1: Percentage of perfectly reconstructed graphs and edit distance. As we were unable to reproduce the results from PIGVAE, these are reported from [12].

DATASET	METRIC	GRALE	PIGVAE*	GRAVITI (AE)	GRAVITI (VAE)
QM9NoHydro	Edit Dist.	0.05	N/A	0.14	0.13
	Accuracy	97.2	N/A	96.3	97.0
PubChem16	Edit Dist.	0.06	1.69*	0.05	0.05
	Accuracy	96.8	41.0*	99.1	99.0
PubChem32	Edit Dist.	0.70	2.53*	0.20	0.14
	Accuracy	73.3	24.9*	97.1	98.3
Coloring w/o ordering	Edit Dist.	0.11	2.13*	35.5	35.3
	Accuracy	95.8	85.3*	0	0
Coloring with ordering	Edit Dist.	0.06	N/A	0.57	0.79
	Accuracy	96.9	N/A	80.5	76.3

5.2 Reconstruction performance

Table 1 reports the graph reconstruction performance of our model using what we consider to be the primary evaluation metric of this study. We deliberately adopt a particularly strict reconstruction criterion, under which a graph is deemed correctly reconstructed only if all node types and all edge types are predicted without error. For molecules, this requirement is further extended to include the exact reconstruction of the hydrogen count and formal charge for every aromatic atom. The reported accuracy therefore corresponds to the proportion of graphs that are perfectly reconstructed. We also report the less strict edit distance [38] for each model. All models are trained until convergence.

We observe the following results: on QM9, where significant overfitting is observed, our model reaches slightly lower performance than GRALE, although comparable. The true difference is on the larger datasets PubChem 16 and 32, where our model beats the baselines by up to 25%. We attribute this success to the increasing difficulty of training a proper matching as graph size increases for GRALE. This demonstrates in particular that the canonical ordering provided in molecular datasets is sufficiently consistent to ensure good performance, especially as graphs get larger, rejoining results observed on readout functions [39].

In order to evaluate the impact of even a basic, yet consistent ordering, we experiment on the COLORING dataset, which does not have such an ordering and should thus be unmanageable for our model. Unsurprisingly, the base results yield a reconstruction accuracy close to 0. We then enforce an ordering on the node, based on WL colors (details in appendix C). The model trained on the dataset with this ordering reaches 80.5% accuracy.

5.3 Ablation studies

To identify the most influential components of our architecture, we perform an ablation study on our best PubChem-16 model in aromatic form, removing or substituting individual modules. The results are reported in Table 2. Overall, the model remains remarkably robust to most modifications. The largest drops in performance arise when replacing the transformer encoder with a message-passing GNN, and when substituting our transformer-based readout with a simple sum pooling. We also observe that cross-entropy unexpectedly outperforms the focal loss in this setting, contrary to the preliminary experiments that initially motivated our choice of focal loss.

As an additional experiment, we trained our model on QM9 using the GRALE loss, reaching 97.9% reconstruction accuracy, surpassing all other models, showing that architecture is fully compatible with permutation-invariant matching objectives and can benefit from them in small-graph settings.

5.4 Other tasks

Denosing Autoencoders are effective tools for denoising structured data. To evaluate this capability, we sample 1024 graphs from PubChem16 and introduce controlled noise by randomly altering node and edge labels, which can include the creation or deletion of edges. We then forward these corrupted graphs through our model. Figure 2 reports the validity of molecules after the noising procedure and after

Table 2: Ablation study results. The baseline model is the VAE on PubChem16, ablated models have the exact same architecture apart from the ablated component.

ABLATED COMPONENT	ALTERNATIVE	ACC.	DIFF.	ED. DIST.	DIFF.
Baseline		99.0	0	0.05	0
Transformer Encoder	GNN-based Enc.	94.1	-4.9	0.21	+0.15
Transformer Readout	Sum-pooling Readout	98.7	-0.3	0.06	+0.01
Trans. Encoder/ Trans.Readout	GNN/Sum-pool	91.9	-7.1	0.34	+0.29
Transformer Decoder	MLP Decoder	98.3	-0.7	0.06	+0.01
Stacking + PE Readin	MLP Readin	98.9	-0.1	0.06	+0.01
Transf. Dec./Stack + PE ReadIn	MLP/MLP	98.3	-0.7	0.06	+0.01
Focal loss	Cross-entropy	99.4	+0.4	0.05	0
Atom attributes Used	Not used	98.4	-0.6	0.07	+0.02
Laplacian + RW Pos. Encoding	Laplacian only	98.8	-0.2	0.06	+0.01
Laplacian + RW Pos. Encoding	RW only	98.9	-0.1	0.05	0
Laplacian + RW Pos. Encoding	None	97.7	-1.3	0.10	+0.05

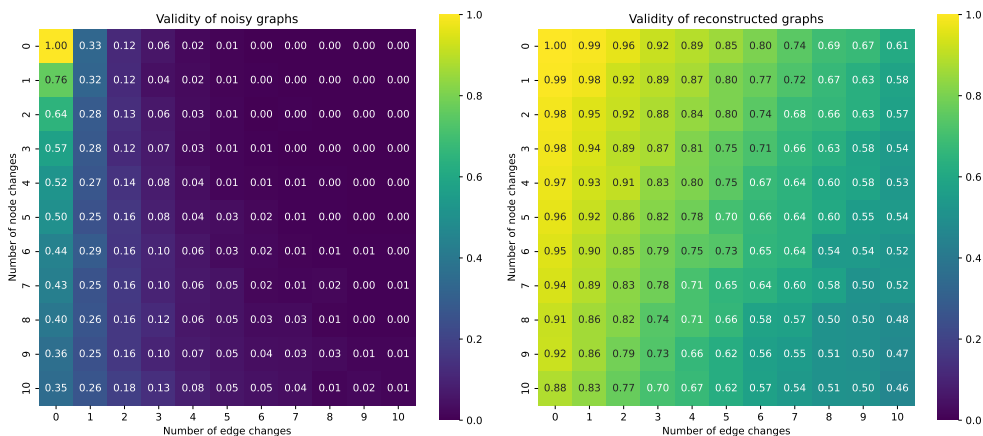


Figure 2: Denoising results: each cell reports the fraction of valid molecules (from PubChem16) after applying a number of random node and edge edits (left) and after reconstruction by the model (right). The VAE consistently restores chemically valid structures even under heavy perturbations.

reconstruction by the autoencoder. The results show a clear improvement in molecular validity once the noisy inputs are passed through the model, confirming its denoising ability, even with large numbers of edits.

Local Property Optimization We demonstrate that our latent embedding can be used not only to represent molecules but also to edit them in a controlled manner to improve a target property. To illustrate this capability, we perform black-box optimization directly in the latent space using CMA-ES [40, 41] to maximize $\log P$ [42, 43], which quantifies the ratio of lipo- over hydro-philicity and is widely sought in drug design. Figure 3 shows representative optimization trajectories.

The results highlight that the latent space supports smooth and minimal structural edits that incrementally improve the objective. CMA-ES parameters enforces small steps between successive candidates, and we observe that the decoded molecules evolve gradually. We also notice the recovery of well-established chemical patterns during optimization. In the left example, the algorithm increases $\log P$ by progressively lengthening the carbon chain. This behavior aligns with a documented principle: longer alkyl chains are increasingly hydrophobic, raising $\log P$ [44, 45, 46, 47]. On the right, the molecule develops a tetrachlorobenzene moiety, another structure associated with increased hydrophobicity [48]. The fact that such trends emerge purely from latent-space navigation suggests that the model captures chemically meaningful directions that can be directly exploited for property-guided molecular editing.

We also note that VAE performs significantly better than AE on this task, with the latter often not finding a near improvement beyond the original embedding, showing the benefits of imposing structure on the latent. On a batch of 1024 molecules, average $\log P$ improvement was 0.16 using AE, and 2.72

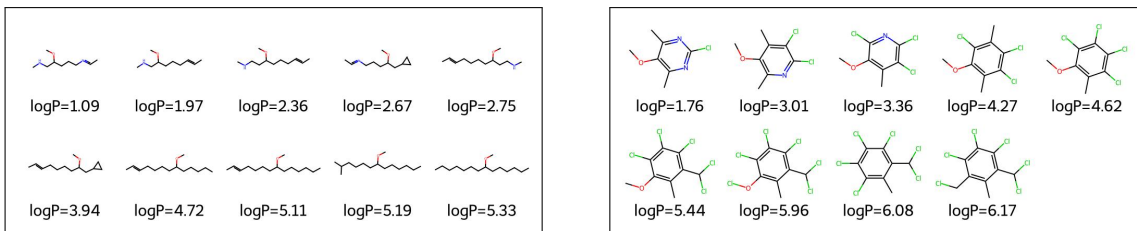


Figure 3: LogP maximization from 2 molecules. Starting from the embedding of the top-left molecule, the latent representation is optimized through CMA-ES to increase its logP (indicated below each molecule). Steps of the optimization are displayed (left-to-right, top to bottom).

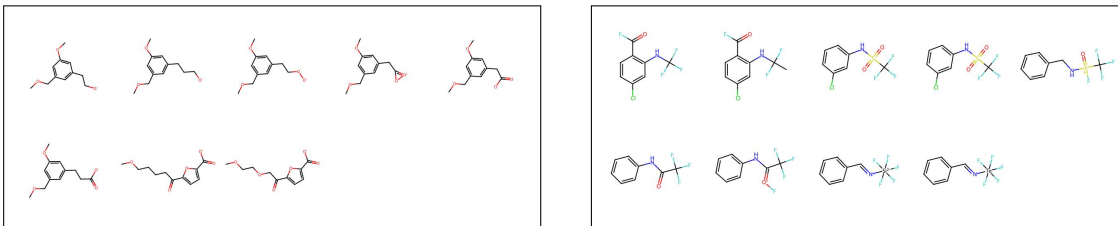


Figure 4: Interpolation between two pairs of molecules (only steps where the molecule is updated are shown). Starting molecules is top-left, progression is left to right, top to bottom.

using VAE. Figure 5 in Appendix D illustrates the performance on individual samples.

Interpolation We also demonstrate that the latent embedding enables smooth transition between two molecules. To illustrate this, we perform linear interpolation directly in latent space between the embeddings of two valid molecules. This produces a continuous trajectory of latent vectors, each of which we decode back into a molecular graph. Because the decoder may map nearby latent points to identical structures, we retain only the distinct molecules encountered along the interpolation. Example interpolations sequences are shown in Figure 4, with more in Appendix F.

Downstream Tasks To evaluate the chemical expressiveness and structural organization of our latent space, we test whether meaningful molecular information can be recovered directly from the embeddings. We embed the QM9 molecules using a model trained on PubChem. Using only the latent vectors as input, we train simple regressors to predict three key molecular properties: dipole moment, HOMO-LUMO gap, and U_0 the 0 K internal energy. These properties probe complementary aspects of molecular structure and chemical behavior. The results are reported in table 3.

To further evaluate whether the latent space captures graph-level information beyond molecular structure, we consider a regression task on Bayesian networks. We use the BN dataset introduced in D-VAE [49], consisting of 200,000 8-node Bayesian networks generated with the bnlearn package [50]. Each graph is assigned a Bayesian Information Criterion (BIC) score measuring how well the network structure fits the Asia dataset [51]. We first train small models for reconstruction (where all models and baseline reach 100% accuracy), and using the encoder embeddings we train MLP regressors to predict the BIC score. The results are reported in table 4.

Table 5: Generation performance on molecular datasets. 10 batches of 1024 molecules are generated, we report mean and std. QM9’s novelty is irrelevant due to QM9 being exhaustive.

DATASET	VALIDITY (%)	UNIQUENESS (%)	NOVELTY (%)
QM9NoHydro (Aromatic)	83.0 \pm 0.89	99.0 \pm 0.30	N/A
QM9NoHydro (Non-Aromatic)	92.6 \pm 0.82	96.3 \pm 0.67	N/A
PubChem16 (Aromatic)	49.9 \pm 1.42	100 \pm 0.00	88.3 \pm 1.65
PubChem16 (Non-Aromatic)	69.2 \pm 1.71	99.8 \pm 0.00	84.69 \pm 0.01

Table 3: Downstream task: regression on molecular properties. MSE is reported (mean and standard deviation over 5 folds). Models are trained either on PubChem16 or 32, as indicated.

MODEL	DIPOLE MOMENT	HOMO-LUMO	ENERGY AT 0 KELVIN
GRALE (PC16)	0.4029 \pm 0.0071	0.1230 \pm 0.0026	0.0033 \pm 0.0010
GRALE (PC32)	0.3677 \pm 0.0105	0.1484 \pm 0.0033	0.0204 \pm 0.0024
GraViti (VAE, PC16)	0.3219 \pm 0.0042	0.0975 \pm 0.0032	0.0056 \pm 0.0001
GraViti (AE, PC16)	0.3322 \pm 0.0016	0.0929 \pm 0.0013	0.0035 \pm 0.0002
GraViti (VAE, PC32)	0.2937 \pm 0.0012	0.0861 \pm 0.0030	0.0106 \pm 0.0053
GraViti (AE, PC32)	0.3040 \pm 0.0096	0.0853 \pm 0.0017	0.0034 \pm 0.0002

Table 4: Downstream task: regression on BIC score. RMSE and Pearson correlation coefficient are reported (mean and standard deviation). Models are trained on BN dataset.

MODEL	RMSE	PEARSON’S r
GRALE	0.0247 \pm 0.0052	0.9997 \pm 0.0001
GraViti (VAE)	0.0457 \pm 0.0021	0.9990 \pm 0.0001
GraViti (AE)	0.0229 \pm 0.0038	0.9997 \pm 0.0001

Graph generation capability Sampling from the latent space of the VAE and applying the decoder allows for straightforward molecule generation. Table 5 shows the generative performance of our models on QM9 and PubChem using standard metrics: validity (percentage of chemically valid generated molecules according to RDKit¹), uniqueness (the percentage of valid molecules that are unique), and novelty (the percentage of unique valid molecules that do not appear in the training set).

Using explicit aromatic representation, we obtain 49.9% validity on PubChem16 and 83% on QM9. A large fraction of invalid molecules contain aromatic edges not forming closed aromatic cycles, reflecting the known difficulty of graph neural networks, including transformers, in representing cyclic structures without higher-order mechanisms [52, 53, 54]. Training the model on the corresponding kekulized representation improves validity to 69% on PubChem and 93% on QM9.

We interpret these results as indicating that the latent space is locally well structured, enabling the generation of diverse and novel molecules in nearby regions, but globally insufficiently compact, leading to a significant fraction of invalid decodings when sampling more broadly. This observation is consistent with the literature on molecular VAEs [55, 56, 57, 58], which has shown that generation validity is commonly low in the absence of additional domain-specific constraints [59, 60].

6 Conclusion and future work

We introduced **GraViti**, a transformer-based graph-level variational autoencoder that learns compact latent representations of entire graphs and achieves state-of-the-art reconstruction accuracy on large graph datasets.

We demonstrate on molecular graphs that the latent space is coherent and chemically meaningful: it supports smooth interpolation, denoising, and property-guided optimization, even recovering known chemical principles. Beyond molecular tasks, we also obtain strong performance on downstream inference problems for Bayesian graphs.

Finally, we show that strict permutation invariance is not always required; when a stable node ordering is available, relaxing this constraint yields substantial gains in reconstruction quality and scalability. Future work includes integrating domain-aware constraints to improve generation validity, exploring richer latent priors, and evaluating transfer to other graph domains such as circuits, proteins, and knowledge graphs. Overall, **GraViti** offers a practical foundation for graph-level representation learning and provides a usable latent space for downstream tasks.

¹RDKit: Open-source cheminformatics. <https://www.rdkit.org>

Acknowledgements

We are grateful to Paul Krzakala, author of [12], for his generous assistance in reproducing the original experiments. Paul’s prompt clarifications and precise technical insights were essential to ensuring a faithful and rigorous comparison.

We also acknowledge that substantial parts of this work were made while the first author was working at KTH, Royal Institute of Technology, Sweden.

J. Lutzeyer is supported by the French National Research Agency (ANR) via the “GraspGNNs” JCJC grant (ANR-24-CE23-3888).

References

- [1] Yoshua Bengio, Aaron Courville, and Pascal Vincent. Representation learning: A review and new perspectives. *IEEE Transactions on Pattern Analysis and Machine Intelligence*, 35(8):1798–1828, 2013.
- [2] Kamal Berahmand, Fatemeh Daneshfar, Elaheh Sadat Salehi, Yuefeng Li, and Yue Xu. Autoencoders and their applications in machine learning: a survey. *Artificial Intelligence Review*, 57(2), February 2024.
- [3] Pengzhi Li, Yan Pei, and Jianqiang Li. A comprehensive survey on design and application of autoencoder in deep learning. *Applied Soft Computing*, 138:110176, 2023.
- [4] Diederik P. Kingma and Max Welling. Auto-Encoding Variational Bayes. In *2nd International Conference on Learning Representations, ICLR 2014, Banff, AB, Canada, April 14-16, 2014, Conference Track Proceedings*, 2014.
- [5] Hadi Vafaii, Dekel Galor, and Jacob L. Yates. Poisson variational autoencoder. In A. Globerson, L. Mackey, D. Belgrave, A. Fan, U. Paquet, J. Tomczak, and C. Zhang, editors, *Advances in Neural Information Processing Systems*, volume 37, pages 44871–44906. Curran Associates, Inc., 2024.
- [6] Thomas N. Kipf and Max Welling. Variational Graph Auto-Encoders. *arXiv:1611.07308 [cs, stat]*, November 2016. arXiv: 1611.07308.
- [7] Kiarash Zahirnia, Oliver Schulte, Parmis Naddaf, and Ke Li. Micro and macro level graph modeling for graph variational auto-encoders. In *Proceedings of the 36th International Conference on Neural Information Processing Systems, NIPS ’22, Red Hook, NY, USA, 2022*. Curran Associates Inc.
- [8] Mohamed Amine Ketata, Nicholas Gao, Johanna Sommer, Tom Wollschläger, and Stephan Günemann. Lift your molecules: Molecular graph generation in latent euclidean space. In *The Thirteenth International Conference on Learning Representations*, 2025.
- [9] Davide Rigoni, Nicolò Navarin, and Alessandro Sperduti. Rgcvae: relational graph conditioned variational autoencoder for molecule design. *Machine Learning*, 114(2), January 2025.
- [10] Fan-Yun Sun, Jordan Hoffman, Vikas Verma, and Jian Tang. Infograph: Unsupervised and semi-supervised graph-level representation learning via mutual information maximization. In *International Conference on Learning Representations*, 2019.
- [11] Robin Winter, Frank Noe, and Djork-Arné Clevert. Permutation-invariant variational autoencoder for graph-level representation learning. In M. Ranzato, A. Beygelzimer, Y. Dauphin, P.S. Liang, and J. Wortman Vaughan, editors, *Advances in Neural Information Processing Systems*, volume 34, pages 9559–9573. Curran Associates, Inc., 2021.
- [12] Paul Krzakala, Gabriel Melo, Charlotte Laclau, Florence d’Alché Buc, and Rémi Flamary. The quest for the GRAPh level autoencoder (GRALE). In *The Thirty-ninth Annual Conference on Neural Information Processing Systems*, 2025.
- [13] Thomas N Kipf and Max Welling. Semi-supervised classification with graph convolutional networks. In *Proceedings of the 5th International Conference on Learning Representations*, 2017.
- [14] Keyulu Xu, Weihua Hu, Jure Leskovec, and Stefanie Jegelka. How Powerful are Graph Neural Networks? In *Proceedings of the 7th International Conference on Learning Representations*, 2019.

- [15] Ashish Vaswani, Noam Shazeer, Niki Parmar, Jakob Uszkoreit, Llion Jones, Aidan N Gomez, Łukasz Kaiser, and Illia Polosukhin. Attention is all you need. In I. Guyon, U. Von Luxburg, S. Bengio, H. Wallach, R. Fergus, S. Vishwanathan, and R. Garnett, editors, *Advances in Neural Information Processing Systems*, volume 30. Curran Associates, Inc., 2017.
- [16] Petar Veličković, Guillem Cucurull, Arantxa Casanova, Adriana Romero, Pietro Liò, and Yoshua Bengio. Graph attention networks. *6th International Conference on Learning Representations*, 2017.
- [17] Yu Rong, Yatao Bian, Tingyang Xu, Weiyang Xie, Ying WEI, Wenbing Huang, and Junzhou Huang. Self-supervised graph transformer on large-scale molecular data. In H. Larochelle, M. Ranzato, R. Hadsell, M.F. Balcan, and H. Lin, editors, *Advances in Neural Information Processing Systems*, volume 33, pages 12559–12571. Curran Associates, Inc., 2020.
- [18] Vijay Prakash Dwivedi and Xavier Bresson. A generalization of transformer networks to graphs. *AAAI Workshop on Deep Learning on Graphs: Methods and Applications*, 2021.
- [19] Luis Müller, Mikhail Galkin, Christopher Morris, and Ladislav Rampásek. Attending to graph transformers. *Transactions on Machine Learning Research*, 2024.
- [20] Devin Kreuzer, Dominique Beaini, Will Hamilton, Vincent Létourneau, and Prudencio Tossou. Rethinking graph transformers with spectral attention. In M. Ranzato, A. Beygelzimer, Y. Dauphin, P.S. Liang, and J. Wortman Vaughan, editors, *Advances in Neural Information Processing Systems*, volume 34, pages 21618–21629. Curran Associates, Inc., 2021.
- [21] Yinan Huang, Haoyu Peter Wang, and Pan Li. What are good positional encodings for directed graphs? In *The Thirteenth International Conference on Learning Representations*, 2025.
- [22] Ladislav Rampásek, Mikhail Galkin, Vijay Prakash Dwivedi, Anh Tuan Luu, Guy Wolf, and Dominique Beaini. Recipe for a general, powerful, scalable graph transformer. In *Proceedings of the 36th International Conference on Neural Information Processing Systems, NIPS '22*, Red Hook, NY, USA, 2022. Curran Associates Inc.
- [23] Dexiong Chen, Leslie O’Bray, and Karsten Borgwardt. Structure-aware transformer for graph representation learning. In *Proceedings of the 39th International Conference on Machine Learning (ICML)*, Proceedings of Machine Learning Research, 2022.
- [24] Rex Ying, Jiaxuan You, Christopher Morris, Xiang Ren, William L. Hamilton, and Jure Leskovec. Hierarchical graph representation learning with differentiable pooling. In *Proceedings of the 32nd International Conference on Neural Information Processing Systems, NIPS'18*, page 4805–4815, Red Hook, NY, USA, 2018. Curran Associates Inc.
- [25] Aditya Grover, Aaron Zweig, and Stefano Ermon. Graphite: Iterative generative modeling of graphs. In Kamalika Chaudhuri and Ruslan Salakhutdinov, editors, *Proceedings of the 36th International Conference on Machine Learning*, volume 97 of *Proceedings of Machine Learning Research*, pages 2434–2444. PMLR, 09–15 Jun 2019.
- [26] Martin Simonovsky and Nikos Komodakis. *GraphVAE: Towards Generation of Small Graphs Using Variational Autoencoders*, page 412–422. Springer International Publishing, 2018.
- [27] Wei Huang, Hanchen Wang, Dong Wen, Shaozhen Ma, Wenjie Zhang, and Xuemin Lin. Towards unsupervised training of matching-based graph edit distance solver via preference-aware GAN. In *The Thirty-ninth Annual Conference on Neural Information Processing Systems*, 2026.
- [28] Xiang Ling, Lingfei Wu, Saizhuo Wang, Tengfei Ma, Fangli Xu, Alex X. Liu, Chunming Wu, and Shouling Ji. Multilevel graph matching networks for deep graph similarity learning. *IEEE Transactions on Neural Networks and Learning Systems*, 34(2):799–813, 2023.
- [29] Clément Vignac, Igor Krawczuk, Antoine Siraudin, Bohan Wang, Volkan Cevher, and Pascal Frossard. Digress: Discrete denoising diffusion for graph generation. In *ICLR*. OpenReview.net, 2023.
- [30] Floor Eijkelboom, Grigory Bartosh, Christian A. Naesseth, Max Welling, and Jan-Willem van de Meent. Variational flow matching for graph generation. In A. Globerson, L. Mackey, D. Belgrave, A. Fan, U. Paquet, J. Tomczak, and C. Zhang, editors, *Advances in Neural Information Processing Systems*, volume 37, pages 11735–11764. Curran Associates, Inc., 2024.

- [31] Tsung-Yi Lin, Priya Goyal, Ross Girshick, Kaiming He, and Piotr Dollár. Focal loss for dense object detection. *IEEE Transactions on Pattern Analysis and Machine Intelligence*, 42(2):318–327, 2020.
- [32] Paul Krzakala, Junjie Yang, Rémi Flamary, Florence d’Alché Buc, Charlotte Laclau, and Matthieu Labeau. Any2graph: Deep end-to-end supervised graph prediction with an optimal transport loss. In *Neural Information Processing Systems (NeurIPS)*, 2024.
- [33] Raghunathan Ramakrishnan, Pavlo O. Dral, Matthias Rupp, and O. Anatole von Lilienfeld. Quantum chemistry structures and properties of 134 kilo molecules. *Scientific Data*, 1(1), August 2014.
- [34] Sunghwan Kim, Paul A. Thiessen, Evan E. Bolton, Jie Chen, Gang Fu, Asta Gindulyte, Lianyi Han, Jane He, Siqian He, Benjamin A. Shoemaker, Jiyao Wang, Bo Yu, Jian Zhang, and Stephen H. Bryant. Pubchem substance and compound databases. *Nucleic Acids Research*, 44(D1):D1202–D1213, 01 2016.
- [35] Chence Shi*, Minkai Xu*, Zhaocheng Zhu, Weinan Zhang, Ming Zhang, and Jian Tang. Graphaf: a flow-based autoregressive model for molecular graph generation. In *International Conference on Learning Representations*, 2020.
- [36] Youzhi Luo, Keqiang Yan, and Shuiwang Ji. Graphdf: A discrete flow model for molecular graph generation. In *International Conference on Machine Learning*, 2021.
- [37] Jaehyeong Jo, Seul Lee, and Sung Ju Hwang. Score-based generative modeling of graphs via the system of stochastic differential equations. In Kamalika Chaudhuri, Stefanie Jegelka, Le Song, Csaba Szepesvari, Gang Niu, and Sivan Sabato, editors, *Proceedings of the 39th International Conference on Machine Learning*, volume 162 of *Proceedings of Machine Learning Research*, pages 10362–10383. PMLR, 17–23 Jul 2022.
- [38] Runzhong Wang, Ziao Guo, Wenzheng Pan, Jiale Ma, Yikai Zhang, Nan Yang, Qi Liu, Longxuan Wei, Hanxue Zhang, Chang Liu, Zetian Jiang, Xiaokang Yang, and Junchi Yan. Pygmtools: A python graph matching toolkit. *Journal of Machine Learning Research*, 25(33):1–7, 2024.
- [39] David Buterez, Jon Paul Janet, Steven J Kiddle, Dino Oglic, and Pietro Liò. Graph neural networks with adaptive readouts. In Alice H. Oh, Alekh Agarwal, Danielle Belgrave, and Kyunghyun Cho, editors, *Advances in Neural Information Processing Systems*, 2022.
- [40] Nikolaus Hansen, Youhei Akimoto, and Petr Baudis. CMA-ES/pycma on Github. Zenodo, DOI:10.5281/zenodo.2559634, February 2019.
- [41] Nikolaus Hansen and Andreas Ostermeier. Completely derandomized self-adaptation in evolution strategies. *Evolutionary Computation*, 9(2):159–195, 2001.
- [42] Daria Klimoszek, Małgorzata Jeleń, Małgorzata Dołowy, and Beata Morak-Młodawska. Study of the lipophilicity and admet parameters of new anticancer diquinothiazines with pharmacophore substituents. *Pharmaceuticals*, 17(6):725, Jun 2024.
- [43] Anna Tsantili-Kakoulidou and Vassilis Demopoulos. Drug-like properties and fraction lipophilicity index as a combined metric. *ADMET and DMPK*, 9(3):177–190, October 2021.
- [44] Anna Mozrzymas. On the hydrophobic chains effect on critical micelle concentration of cationic gemini surfactants using molecular connectivity indices. *Monatshefte für Chemie - Chemical Monthly*, 151(4):525–531, April 2020.
- [45] Rong Yang, Xiaojuan Lai, Qiying Li, Xi Ding, Lei Wang, Xin Wen, and Yan Guo. Effect of hydrophobic monomers with different carbon chains on the structure–activity relationship of associating polyacrylamides. *Journal of Polymer Research*, 31(242), Jul 2024.
- [46] Zhang Xie, Zheng Li, Gang Lou, Qing Liang, Jiang-Xing Chen, Jianlong Kou, and Gui-Na Wei. Interface water-induced hydrophobic carbon chain unfolding in water. *Communications in Theoretical Physics*, 73(5):055602, mar 2021.
- [47] R. Smith and C. Tanford. Hydrophobicity of long chain n-alkyl carboxylic acids, as measured by their distribution between heptane and aqueous solutions. *Proceedings of the National Academy of Sciences of the United States of America*, 70(2):289–293, February 1973.

- [48] Kerry N. McPhedran, Rajesh Seth, and Ken G. Drouillard. Hydrophobic organic compound (hoc) partitioning behaviour to municipal wastewater colloidal organic carbon. *Water Research*, 47(7):2222–2230, 2013.
- [49] Muhan Zhang, Shali Jiang, Zhicheng Cui, Roman Garnett, and Yixin Chen. D-vae: A variational autoencoder for directed acyclic graphs, 2019.
- [50] Marco Scutari. Learning bayesian networks with the bnlearn r package. *Journal of Statistical Software*, 35(3):1–22, 2010.
- [51] S. L. Lauritzen and D. J. Spiegelhalter. Local computations with probabilities on graphical structures and their application to expert systems. *Journal of the Royal Statistical Society: Series B (Methodological)*, 50(2):157–194, 01 1988.
- [52] Wenhao Zhu, Tianyu Wen, Guojie Song, Liang Wang, and Bo Zheng. On structural expressive power of graph transformers. In *Proceedings of the 29th ACM SIGKDD Conference on Knowledge Discovery and Data Mining*, KDD '23, page 3628–3637, New York, NY, USA, 2023. Association for Computing Machinery.
- [53] Luis Müller and Christopher Morris. Aligning transformers with weisfeiler-leman. In *Proceedings of the 41st International Conference on Machine Learning*, ICML'24. JMLR.org, 2024.
- [54] Giannis Nikolentzos, Dimitrios Kelesis, and Michalis Vazirgiannis. On the theoretical expressive power of graph transformers for solving graph problems. *Neural Networks*, 194:108112, 2026.
- [55] Matt J. Kusner, Brooks Paige, and José Miguel Hernández-Lobato. Grammar variational autoencoder. In *Proceedings of the 34th International Conference on Machine Learning - Volume 70*, ICML'17, page 1945–1954. JMLR.org, 2017.
- [56] Wengong Jin, Regina Barzilay, and Tommi Jaakkola. Junction tree variational autoencoder for molecular graph generation. In Jennifer Dy and Andreas Krause, editors, *Proceedings of the 35th International Conference on Machine Learning*, volume 80 of *Proceedings of Machine Learning Research*, pages 2323–2332. PMLR, 10–15 Jul 2018.
- [57] Trieu Nguyen and Aleksandra Karolak. Transformer graph variational autoencoder for generative molecular design. *Biophysical Journal*, 124(22):3867–3875, 2025.
- [58] Chao Hu, Song Li, Chenxing Yang, Jun Chen, Yi Xiong, Guisheng Fan, Hao Liu, and Liang Hong. ScaffoldGVAE: scaffold generation and hopping of drug molecules via a variational autoencoder based on multi-view graph neural networks. *J. Cheminform.*, 15(1):91, October 2023.
- [59] Arun Singh Bhadwal, Monika Kumari, and Anil Kumar. Pcf-vae: posterior collapse free variational autoencoder for de novo drug design. *Scientific Reports*, 15(1), October 2025.
- [60] Toshiaki Ochiai, Tensei Inukai, Manato Akiyama, Kairi Furui, Masahito Ohue, Nobuaki Matsumori, Shinsuke Inuki, Motonari Uesugi, Toshiaki Sunazuka, Kazuya Kikuchi, Hideaki Kakeya, and Yasubumi Sakakibara. Variational autoencoder-based chemical latent space for large molecular structures with 3d complexity. *Communications Chemistry*, 6(1), November 2023.

A Statistics of the datasets

Table 6: Statistics of the used datasets.

Name	# Graph	Avg nb of nodes	Avg nb of edges	Max Size	Node types
QM9NoHydro	130k	8.79	9.4	9	4
PubChem16	12.89M	13.87	14.19	16	31
PubChem32	74.34M	21.75	21.15	32	31
Coloring	320k	12.51	24.93	20	4
Asia (BN)	200k	8	8.05	8	8

B Loss function

B.1 Reconstruction Loss

The reconstruction loss is defined over nodes, edges and predicted size. Since both nodes and edges take discrete values (atom and bond types), we treat our graph prediction task as multiple classification tasks, one per node and edge. Because we face a widely unequal distribution of classes, with some elements appearing orders of magnitude more often than others, we use the focal loss, an extension of cross-entropy specifically designed to handle such imbalances:

$$\mathcal{L}_{\text{focal}}(p_t) = -(1 - p_t)^\gamma \log(p_t)$$

with p_t the predicted probability of true class t . The focal loss [31] can also admit class-specific weights, but we find that it performs well on its own, with inverse-frequency weight degrading the performance. For a graph with N nodes, with t_i the class of the i th node and $c_{i,j}$ the class of the edge between nodes i and j , we therefore have:

$$\mathcal{L}_{\text{node}} = \frac{1}{N} \sum_{i=1}^N \mathcal{L}_{\text{focal}}(p_{t_i}^i) \text{ and } \mathcal{L}_{\text{edge}} = \frac{1}{N} \sum_{i=1}^N \sum_{j=1}^N \mathcal{L}_{\text{focal}}(c_{t_i,j}^{i,j})$$

In order to avoid the overwhelmingly frequent “no-edge” class from hurting the training, we actually sample a number of “no-edge” class equal to rN_e , with r a hyperparameter and N_e the number of actual edges.

A natural concern is that this loss is applied in the input node order, which makes it highly sensitive to permutations. As we show in the section 5, this inductive bias is beneficial for dataset with a consistent canonical ordering: enforcing a consistent ordering improves reconstruction fidelity and does not hinder the model’s ability to represent graphs up to isomorphism. Finally, the error $\mathcal{L}_{\text{size}}$ on the predicted log-size \hat{s} is simply the smooth $L1$ error with the real log-size s . Our final reconstruction loss is a combination of those three losses:

$$\mathcal{L}_{\text{rec}} = \mathcal{L}_{\text{node}} + \eta \mathcal{L}_{\text{edge}} + \mathcal{L}_{\text{size}} \text{ with } \eta \text{ a hyperparameter.}$$

B.2 Variational loss

For the latent variables we assume a standard normal prior $\mathcal{N}(0, I)$. Given encoder outputs z_μ and z_σ , the variational term corresponds to the KL divergence between the approximate posterior $q(z | x) = \mathcal{N}(z_\mu, \text{diag}(z_\sigma^2))$ and the prior:

$$\mathcal{L}_{\text{KL}} = D_{\text{KL}}(\mathcal{N}(z_\mu, \text{diag}(z_\sigma^2)) \| \mathcal{N}(0, I)) = -\frac{1}{2} \sum_{i=1}^d (1 + \log z_{\sigma,i}^2 - z_{\mu,i}^2 - z_{\sigma,i}^2).$$

The final training objective is therefore:

$$\mathcal{L} = \mathcal{L}_{\text{rec}} + \beta \mathcal{L}_{\text{KL}},$$

where β optionally controls the strength of the variational term. In practice, β follows a warmup schedule, sinusoidally increasing until plateauing at its maximum value.

C Ordering imposed on COLORING

To demonstrate the importance of ordering for our model, we also run an ablation study on the COLORING dataset [32]. This dataset contains general graphs with only node classes, and such that two nodes of the same color cannot be connected. As such, there is no inherent ordering of the node. To enforce ordering on a Coloring graph $G = (V, E)$, we replace the arbitrary node order with a deterministic WL-based order. Let c_v the sampled color label of node v . We initialize the WL labels as $h_v^{(0)} = c_v$. For $t = 1, 2, 3$, each node receives the signature

$$s_v^{(t)} = \left(h_v^{(t-1)}, \text{sort} \left(h_u^{(t-1)} : u \in N(v) \right) \right),$$

where $N(v)$ is the set of graph neighbors of v . The set of signatures is then compressed into integer labels $h_v^{(t)}$ by sorting the unique signatures lexicographically and assigning consecutive IDs. Thus, after three iterations, $h_v^{(3)}$ encodes the color and topology of the node’s local neighborhood up to radius three, as distinguished by 1-WL refinement.

The final node order is obtained by sorting nodes lexicographically using the tuple

$$\left(h_v^{(3)}, d_r(v), d_a(v), \text{deg}(v), y_v, x_v \right),$$

where $d_r(v), d_a(v)$ are the unweighted shortest-path distances from selected root and anchor nodes, $\text{deg}(v)$ is the graph degree, and (x_v, y_v) is the geometric position of the node.

The root r is chosen as the smallest structurally identifiable node after WL refinement, i.e. the node minimizing

$$\left(h_v^{(3)}, \text{deg}(v), y_v, x_v \right)$$

The anchor a is chosen far from the root to further break symmetries by adding a second axis, as the node maximizing

$$\left(d_r(v), \text{deg}(v), -h_v^{(3)} \right)$$

D Latent optimization of LogP

We show below some extra examples for optimizing logP as described in section 5.4 .

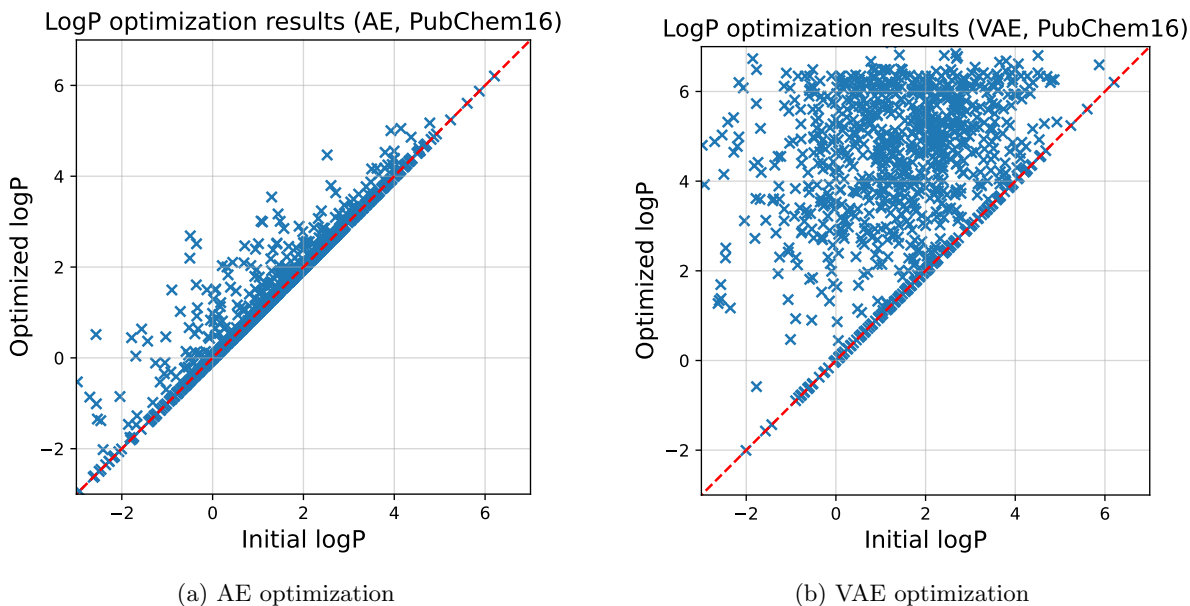


Figure 5: Comparison of AE and VAE optimization performance on 128 random molecules. The structure in the VAE latent allows significantly better improvement.

CMA-ES is obtained from the `cma` package ² run for 100 steps, with `sigma0` set to 0.25, 50 iterations, and a population size of 16.

²<https://pypi.org/project/cma/>

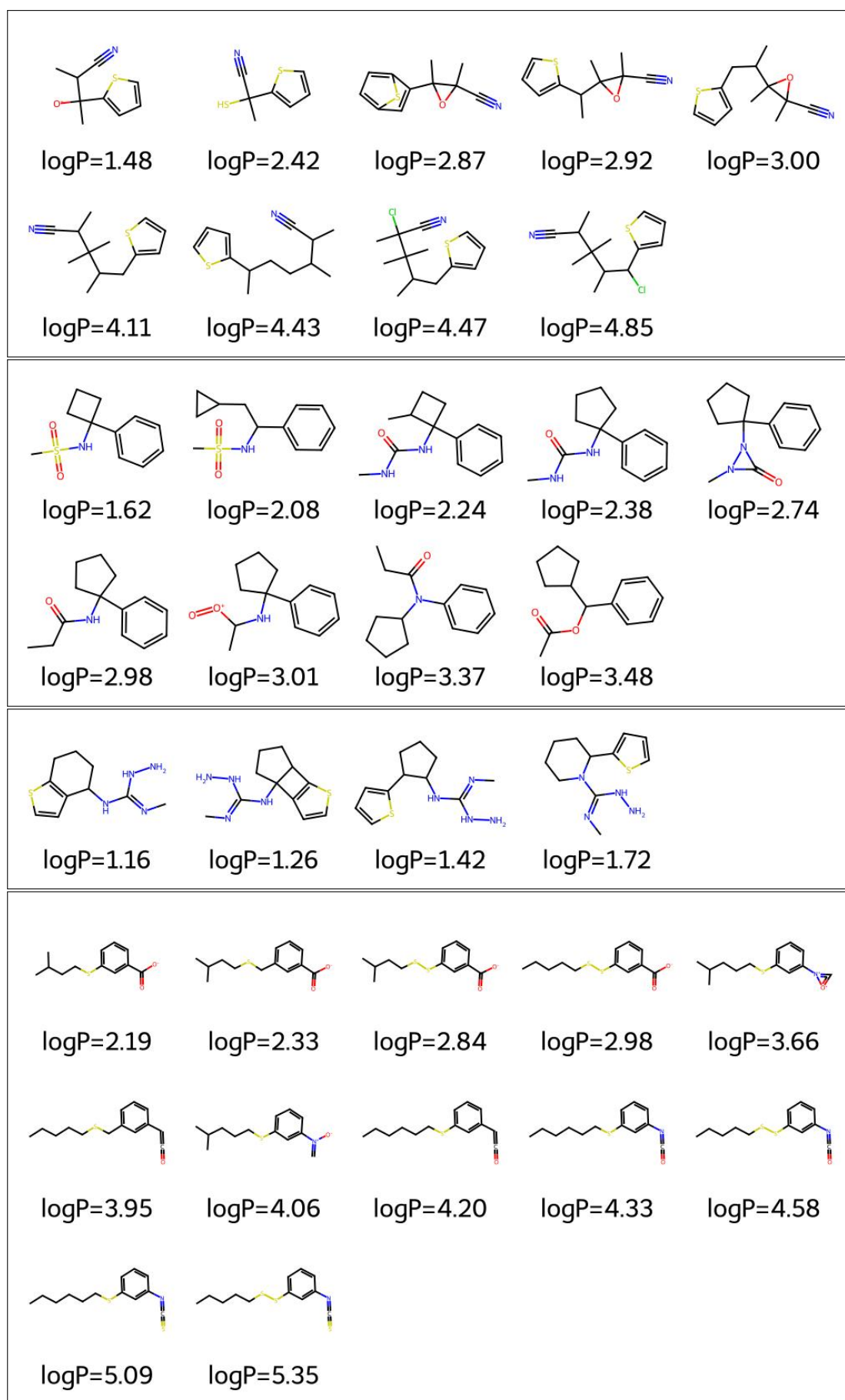


Figure 6: Extra logP optimization plots (PubChem16).

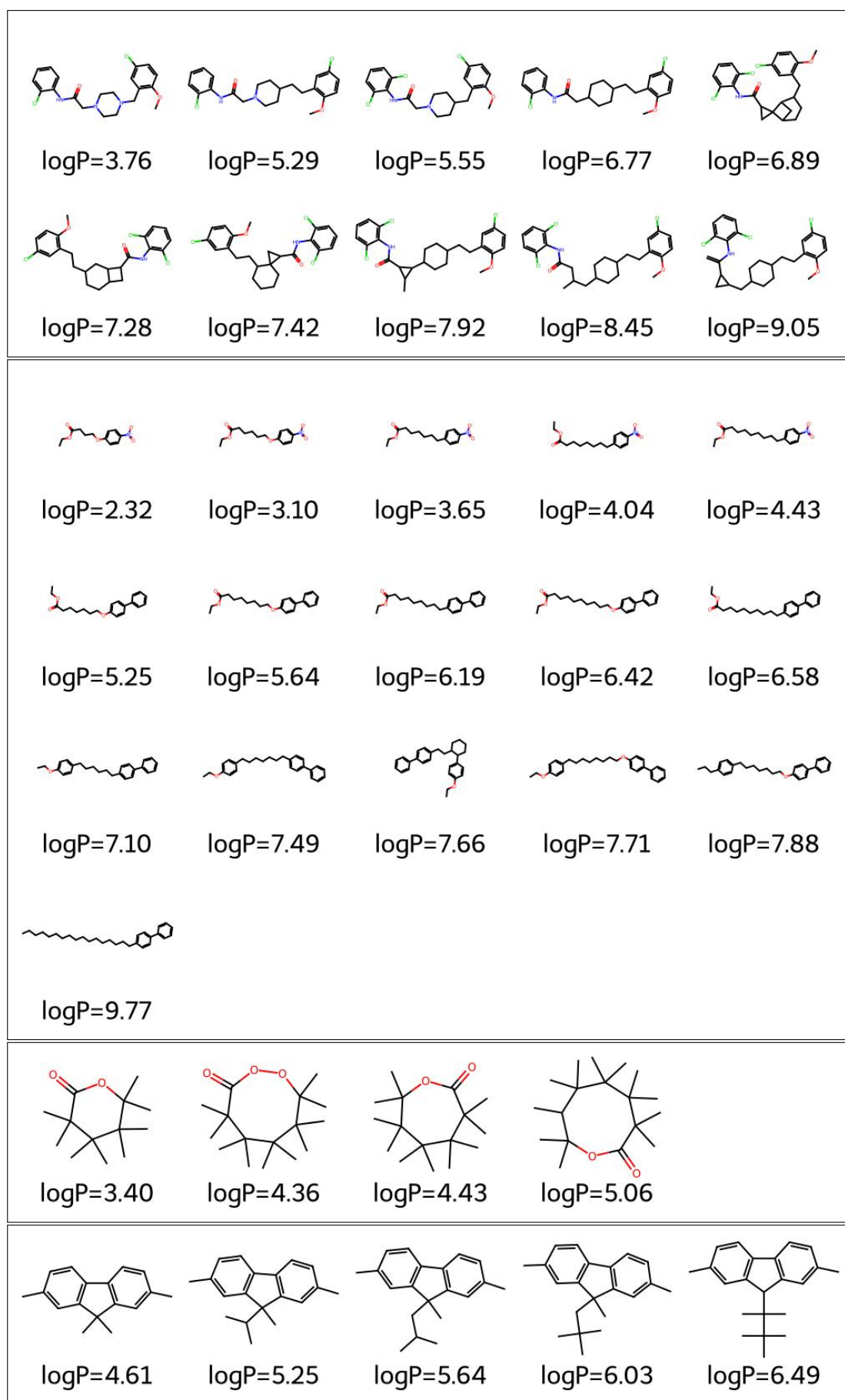


Figure 7: Extra logP optimization plots (PubChem32).

E Denoising: model comparison

Fig. 9 compares the denoising abilities of AE (top) and VAE (bottom), showing a slight advantage for the variational model.

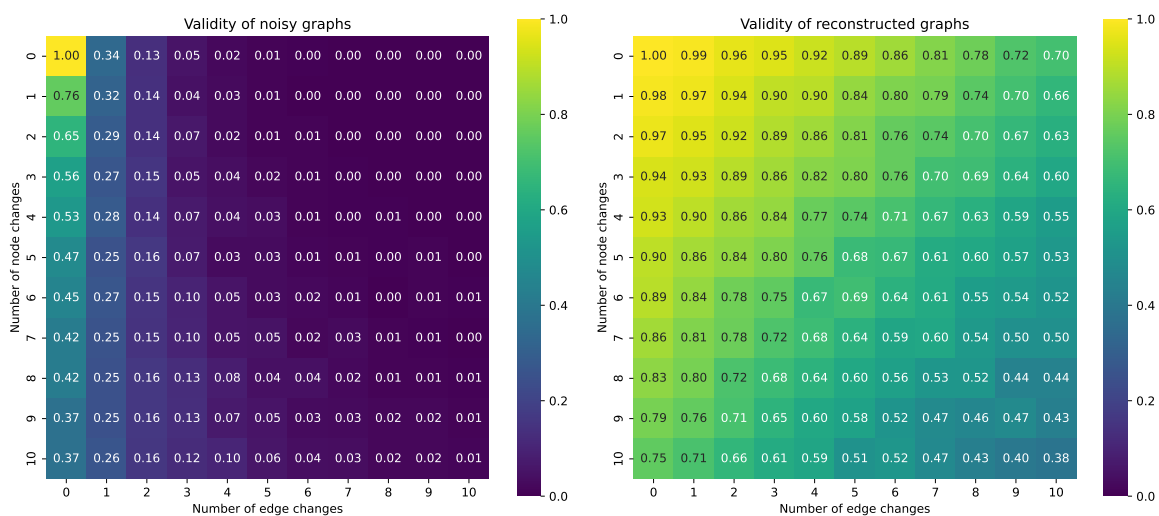


Figure 8: Denoising results: each cell reports the fraction of valid molecules (1024 molecules from PubChem16) after applying a number of random node and edge edits (left) and after reconstruction by the model (right). The AE consistently restores chemically valid structures even under heavy perturbations.

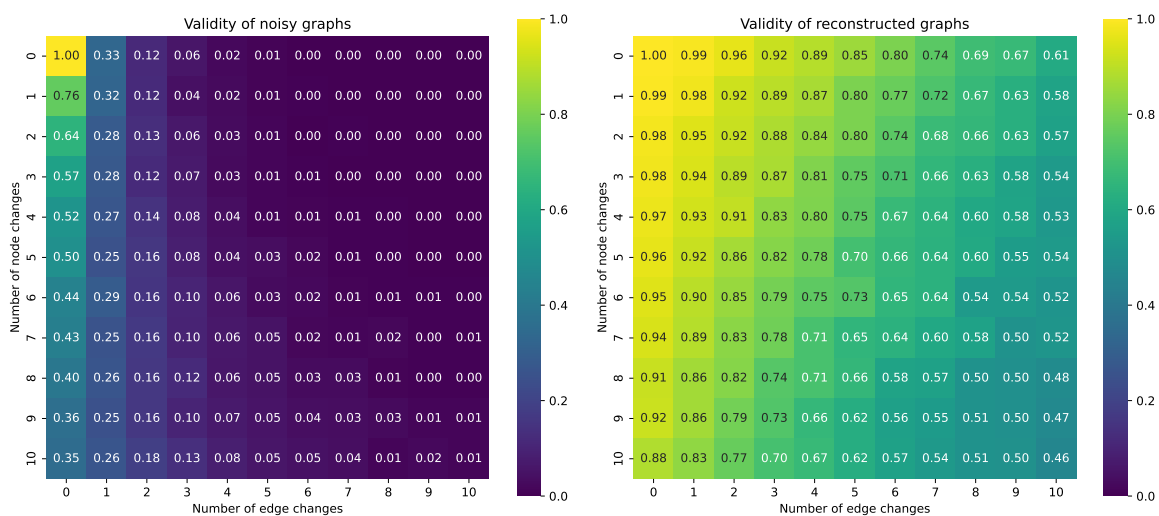
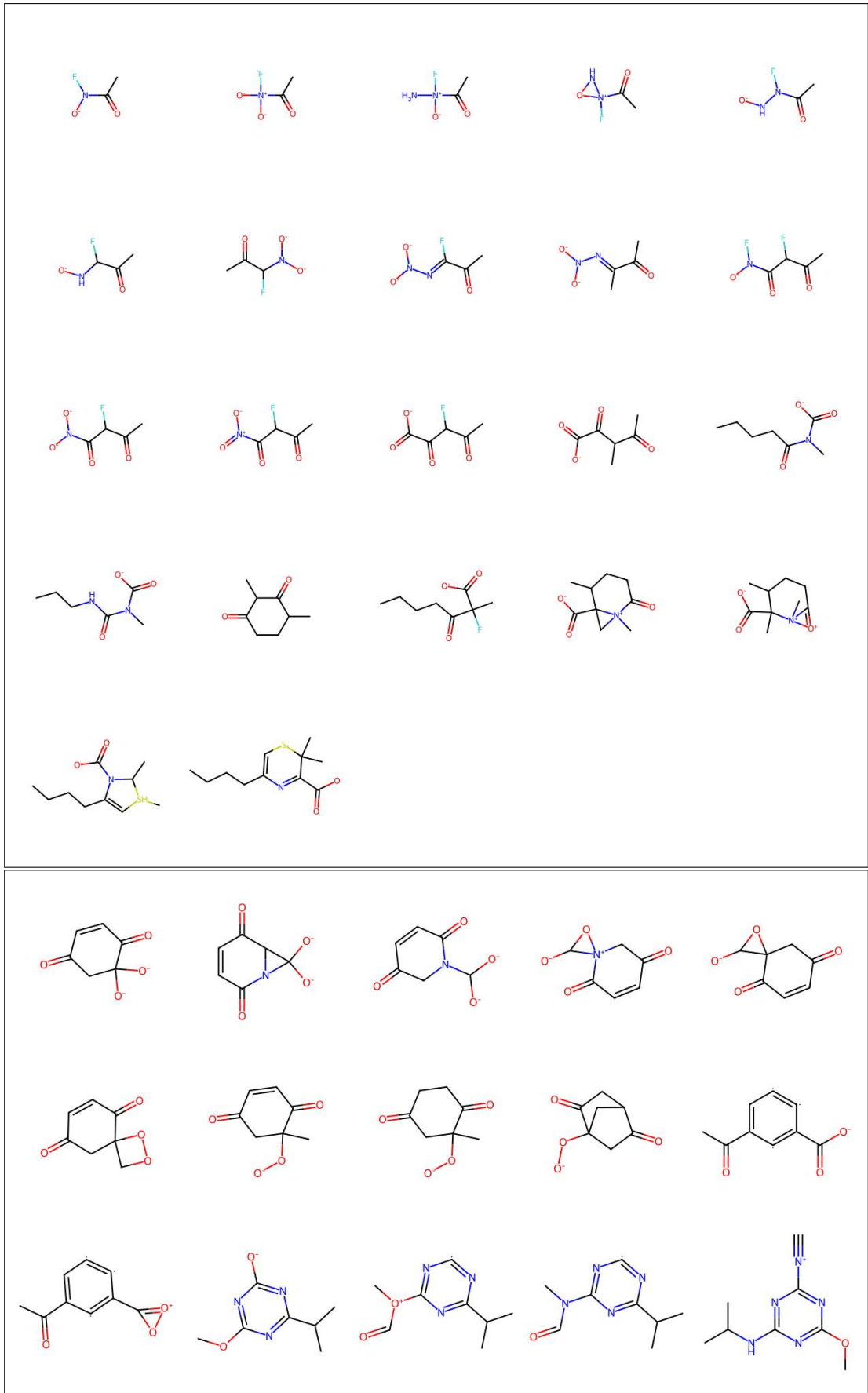


Figure 9: Denoising results: each cell reports the fraction of valid molecules (1024 molecules from PubChem16) after applying a number of random node and edge edits (left) and after reconstruction by the model (right). The VAE consistently restores chemically valid structures even under heavy perturbations.

F Molecule interpolation

We show below some extra examples for molecule interpolation [5.4](#)



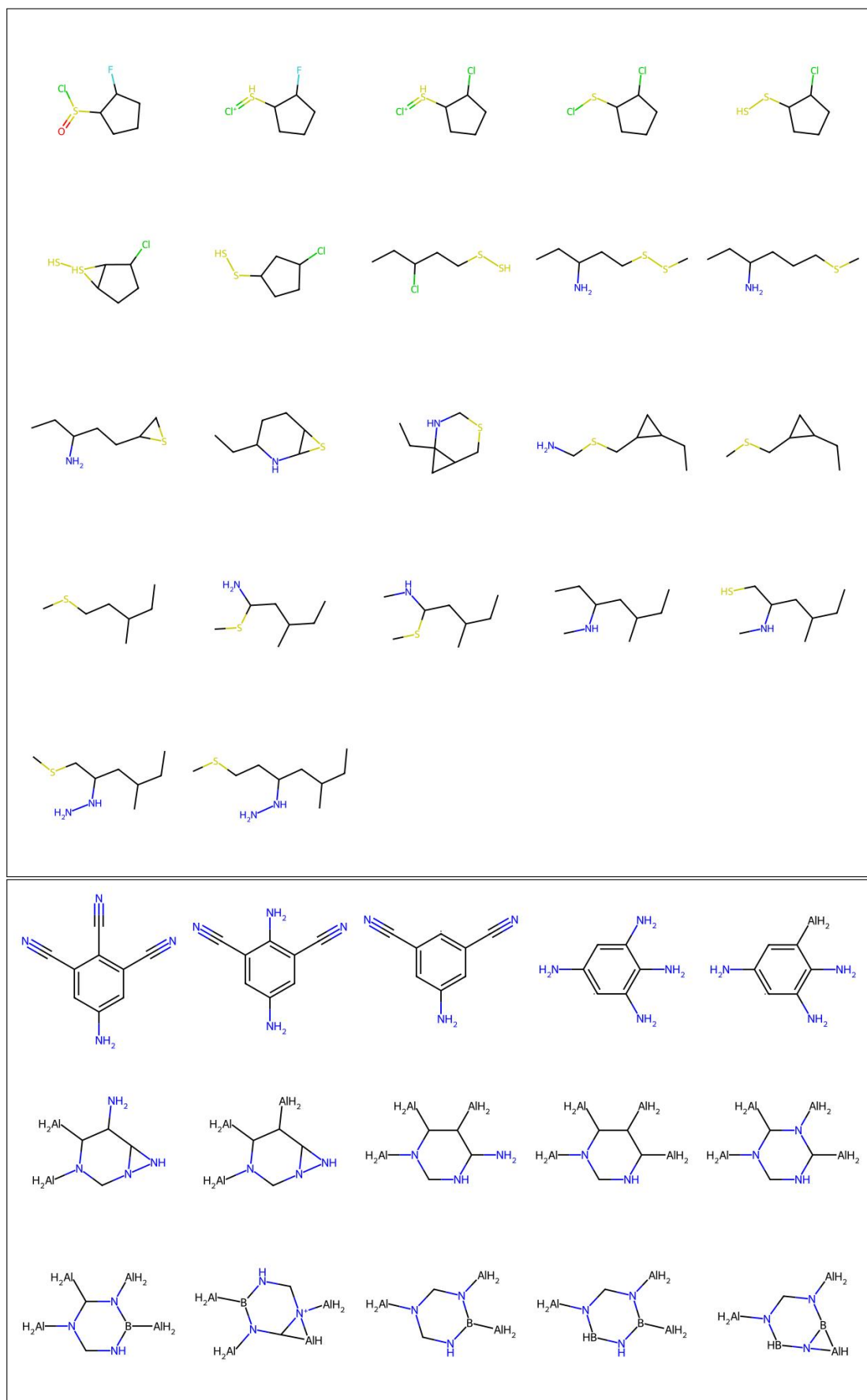


Figure 10: Extra molecule interpolation plots (PC16)

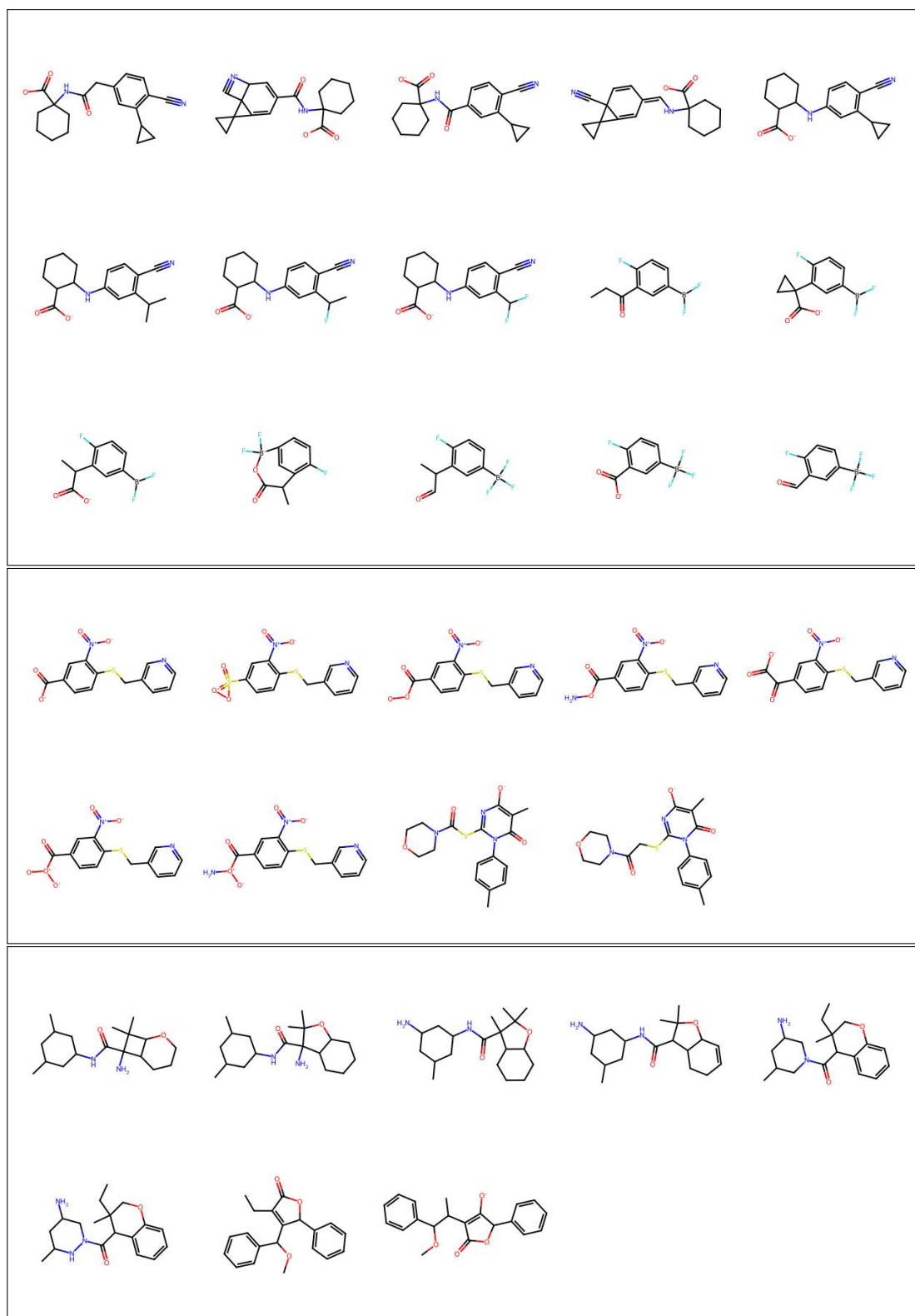


Figure 11: Extra molecule interpolation plots (PC32)

G Generated molecules samples

Figure 12 presents examples of molecules generated by our PubChem-trained model. Latent vectors are sampled from the standard normal prior and decoded into molecular graphs. We report only valid generations, that is, molecules for which all chemical constraints are satisfied.

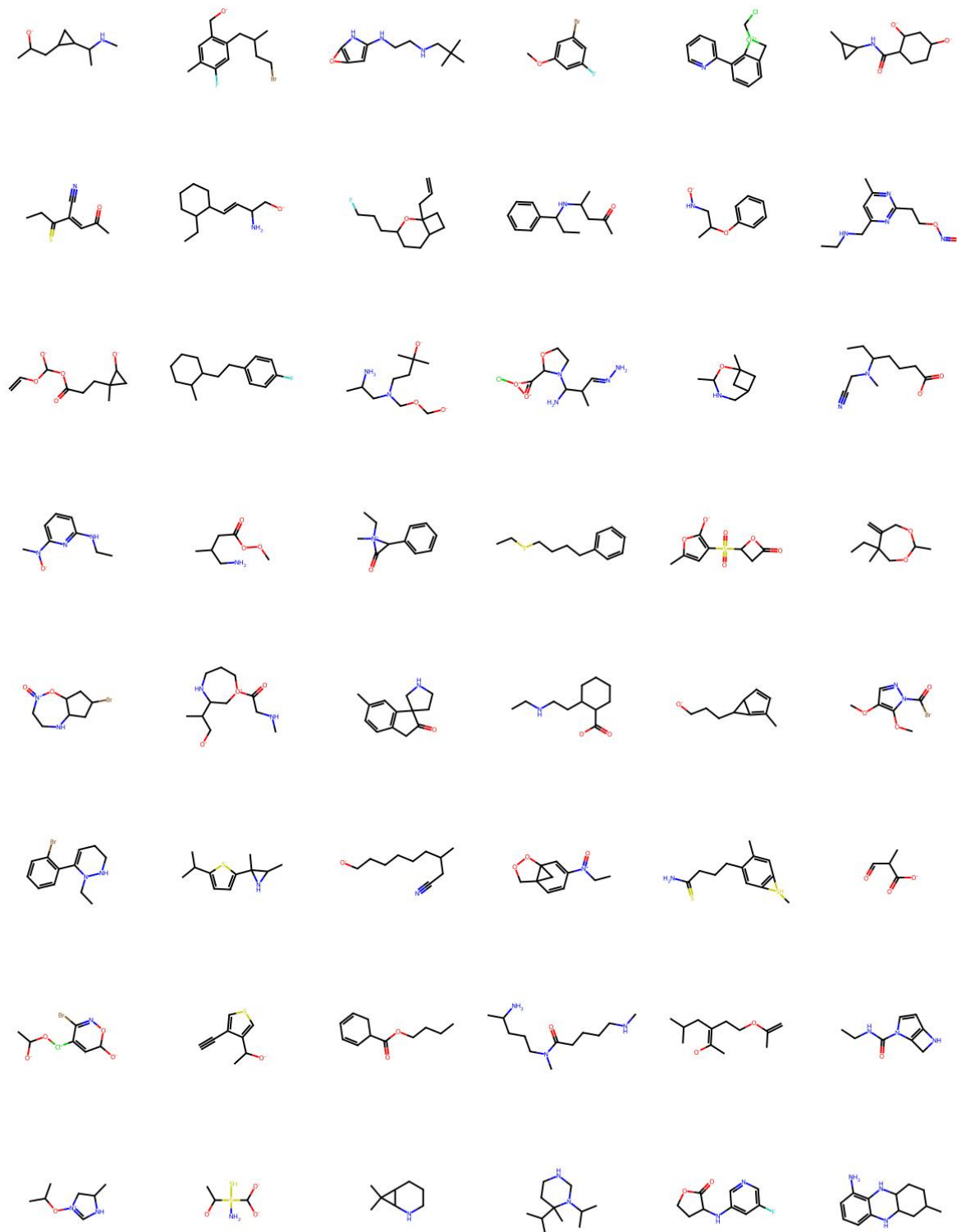


Figure 12: Samples of generated molecules (PubChem16)

H Hyperparameters and training details

We provide in table 7 the hyperparameters used to train our models. Our models use a half-sinusoidal warmup curve for beta (KL-divergence) and a cosine annealing scheduler with warmup and restarts.

Table 7: Hyperparameters used for best models. All experiments were conducted on AMD MI210 GPUs.

Dataset	QM9	PubChem16	PubChem32	Coloring	Asia (BN)
Optimizer	AdamW	AdamW	AdamW	AdamW	AdamW
Learning rate	2e-4	1e-4	1e-4	1e-4	1e-4
Batch size	64	64	256	64	64
Latent dimension	64	256	512	128	64
Encoder hidden size	128	512	512	256	64
Encoder input size	128	128	128	128	64
Graph transformer layers	2	5	7	3	1
Transformer heads	4	4	8	4	1
Beta (VAE)	1e-5	1e-4	1e-5	1e-4	1e-3
LR cycle length	200	200	800	300	30
Beta cycle length	400	200	800	200	30
Ratio negative edges	4	4	4	4	4
Edge loss weight	1.25	1.25	1.25	1	1
Train split	0.8	0.9736	0.9978	0.9375	0.9
Valid. split	0.1	0.003	0.0011	0.03125	0.05
Test. split	0.1	0.0234	0.0011	0.03125	0.05
GPUs (training)	1	1	2	1	1
GPUs (inference)	1	1	1	1	1